

Intersatellite laser ranging instrument for the GRACE follow-on mission

B. S. Sheard · G. Heinzel · K. Danzmann ·
D. A. Shaddock · W. M. Klipstein · W. M. Folkner

Received: 2 November 2011 / Accepted: 16 April 2012 / Published online: 8 May 2012
© Springer-Verlag 2012

Abstract The Gravity Recovery and Climate Experiment (GRACE) has demonstrated that low–low satellite-to-satellite tracking enables monitoring the time variations of the Earth’s gravity field on a global scale, in particular those caused by mass-transport within the hydrosphere. Due to the importance of long-term continued monitoring of the variations of the Earth’s gravitational field and the limited lifetime of GRACE, a follow-on mission is currently planned to be launched in 2017. In order to minimise risk and the time to launch, the follow-on mission will be basically a rebuild of GRACE with microwave ranging as the primary instrument for measuring changes of the intersatellite distance. Laser interferometry has been proposed as a method to achieve improved ranging precision for future GRACE-like missions and is therefore foreseen to be included as demonstrator experiment in the follow-on mission now under development. This paper presents the top-level architecture of an

interferometric laser ranging system designed to demonstrate the technology which can also operate in parallel with the microwave ranging system of the GRACE follow-on mission.

Keywords GRACE · Intersatellite ranging · Laser interferometry

1 Introduction

The Gravity Recovery and Climate Experiment (GRACE) has successfully demonstrated the use of intersatellite ranging between two satellites in low-Earth orbit for monitoring of the spatial and time variable of Earth’s gravity field (Tapley et al. 2003, 2004b). The spatial structure of the Earth’s gravitational field is estimated from the measurements obtained from the two satellites each month. These monthly gravity fields exhibit both seasonal variations and long-term trends. Temporal variations associated with mass transport within the hydrosphere have been identified, see for e.g. Tapley et al. (2004a), Schmidt et al. (2008), Wouters et al. (2008), van den Broeke et al. (2009) and Tiwari et al. (2009). Long-term monitoring of the changing gravitational field of the Earth is of particular importance in order to study the processes driving the observed changes.

GRACE consists of two identical satellites in circular polar orbits. Although the orbit is nominally freely decaying and therefore does not have a constant repeating ground-track pattern (Tapley et al. 2004b), the satellite separation is maintained between 170 and 270 km by occasional orbit maintenance manoeuvres. The intersatellite distance variations induced by the differential accelerations on the two satellites in orbit are measured using a two-way microwave link (Dunn et al. 2003). Two frequencies 24 GHz (K-band) and 32 GHz (Ka band) are used to enable the removal of

B. S. Sheard (✉) · G. Heinzel · K. Danzmann
Max Planck Institute for Gravitational Physics (Albert Einstein Institute) and Institute for Gravitational Physics,
Leibniz Universität Hannover, Callinstrasse 38,
30167 Hanover, Germany
e-mail: benjamin.sheard@aei.mpg.de

G. Heinzel
e-mail: gerhard.heinzel@aei.mpg.de

K. Danzmann
e-mail: karsten.danzmann@aei.mpg.de

D. A. Shaddock
Department of Quantum Science, The Australian
National University, Building 38a, Science Rd.,
Acton, ACT 0200, Australia
e-mail: daniel.shaddock@anu.edu.au

W. M. Klipstein · W. M. Folkner
Jet Propulsion Laboratory, California Institute of Technology,
4800 Oak Grove Drive, Pasadena, CA 91109, USA

variable ionospheric delays. It is important to note that the two satellites effectively comprise a single measurement system.

Estimates of the gravity field are derived from observations obtained from a range of on-board instruments. In addition to the microwave ranging system each satellite includes an accelerometer (Touboul et al. 1999) placed at the spacecraft center of mass which is used to correct for range changes caused by non-gravitational forces acting on the satellites, primarily drag forces from the residual atmosphere and solar radiation. Attitude information obtained from the on-board star cameras is used to correct the ranging data for pointing-induced noise that couples due to the microwave transceiver being located at the front of the spacecraft (see for e.g. Horwath et al. (2011)). Data obtained from the on-board GPS receivers enable precise determination of the satellite orbits and accurate time tagging of the data. The GPS data also contribute to the large spatial scale components of the gravity field (Bertiger et al 2002).

One significant challenge is the removal of the temporal variations of the Earth's gravitational field with periods shorter than one month which are aliased due to under-sampling (Knudsen and Andersen 2002; Seo et al. 2008; Loomis et al. 2011). These high frequency variations can be caused by tides (Visser et al. 2010) and also non-tidal variations, for e.g. associated with mass transport within the atmosphere, oceans and continental hydrology (Thompson et al. 2004). In addition to improving the models used for dealiasing (Zenner et al. 2010), different orbits and multiple satellite pairs (Sneeuw et al. 2005; Bender et al. 2008; Wiese et al. 2009) have been proposed to reduce the effect of aliasing for future missions.

For future gravity field missions not only long-term monitoring but also improved precision is of interest. The design sensitivity for GRACE is limited by the accelerometer noise for frequencies between the orbit frequency ($\approx 200 \mu\text{Hz}$) and a few millihertz, whilst above a few millihertz the microwave system noise, primarily thermal noise in the receiver, dominates (see for e.g. Thomas (1999)). Future gravity field missions based on intersatellite ranging may achieve improved ranging performance using interferometric laser ranging instead of microwave ranging. The higher accuracy is possible with the laser system primarily because of the reduction in operating wavelength by a factor of approximately 10,000 compared to the microwave ranging system. Improved ranging measurement accuracy will allow the ability to measure smaller changes in water mass for a given spatial scale, or allow improved spatial resolution for a given mass change uncertainty. Another consequence of using a smaller wavelength is tighter requirements for beam pointing because of the lower divergence.

GRACE was launched in March 2002 with a design life of 5 years. The mission was subsequently extended until the

end of its on-orbit life. In order to continue the observation of the spatial and temporal variations of the Earth's gravitational field a GRACE follow-on mission is currently being developed and is presently planned to be launched in 2017. In order to minimise the length of the data gap, the follow-on mission will be a close rebuild of the original GRACE design. Although the prime intersatellite ranging instrument for the follow-on mission will be the same microwave ranging system used on GRACE, the mission is an opportunity to include a technology demonstration of a laser ranging instrument (LRI). There is significant technology overlap between the laser ranging demonstrator and the Laser Interferometer Space Antenna (LISA), a space-based gravitational wave detector under development (Danzmann and the LISA Science Team 2003; Danzmann and Rüdiger 2003; Heinzel et al. 2006; Shaddock 2008), from which the proposed instrument derives a number of key technologies. This paper presents the current conceptual design of the demonstration LRI.

2 Laser ranging instrument architecture

The addition of an interferometric laser ranging demonstration instrument is complicated by the fact that its design must be adapted to the existing spacecraft platform design. Ideally, the axis connecting the two reference points of the accelerometers on the two spacecraft would be used for the optical axis as this reduces the coupling from spacecraft attitude jitter into measured pathlength. Placing the limiting aperture of the optical system as close as possible to the accelerometer would further reduce the coupling. Unfortunately, this option is not available for the proposed GRACE follow-on mission as this axis is blocked by the microwave ranging system and also by the cold gas propulsion system fuel tanks. Figure 1 shows the proposed beam routing solution which allows an off-axis system to be used without leading to a significant increase in the sensitivity to spacecraft attitude jitter that would be present if the interferometer axis would simply be shifted to one-side. Due to the shape of this layout it is sometimes referred to as a 'racetrack' configuration.

A key element of this design is the system of three mirrors on each spacecraft, called the triple mirror assembly (TMA), which is used to route the beam path around the cold gas fuel tank (not shown in Fig. 1) and the microwave ranging assembly at the front of the spacecraft. These three mirrors form a corner cube configuration, i.e. the three mirror planes are perpendicular with respect to each other. For small rotations of the device the motion of the beam spots is quite small and the structure does not need to be a complete corner cube—only the surfaces where the beams reflect from need to be physically present. This arrangement has a number of special properties that are useful. First, the intersection point of the three mirror planes (the vertex of the retro-reflector) can

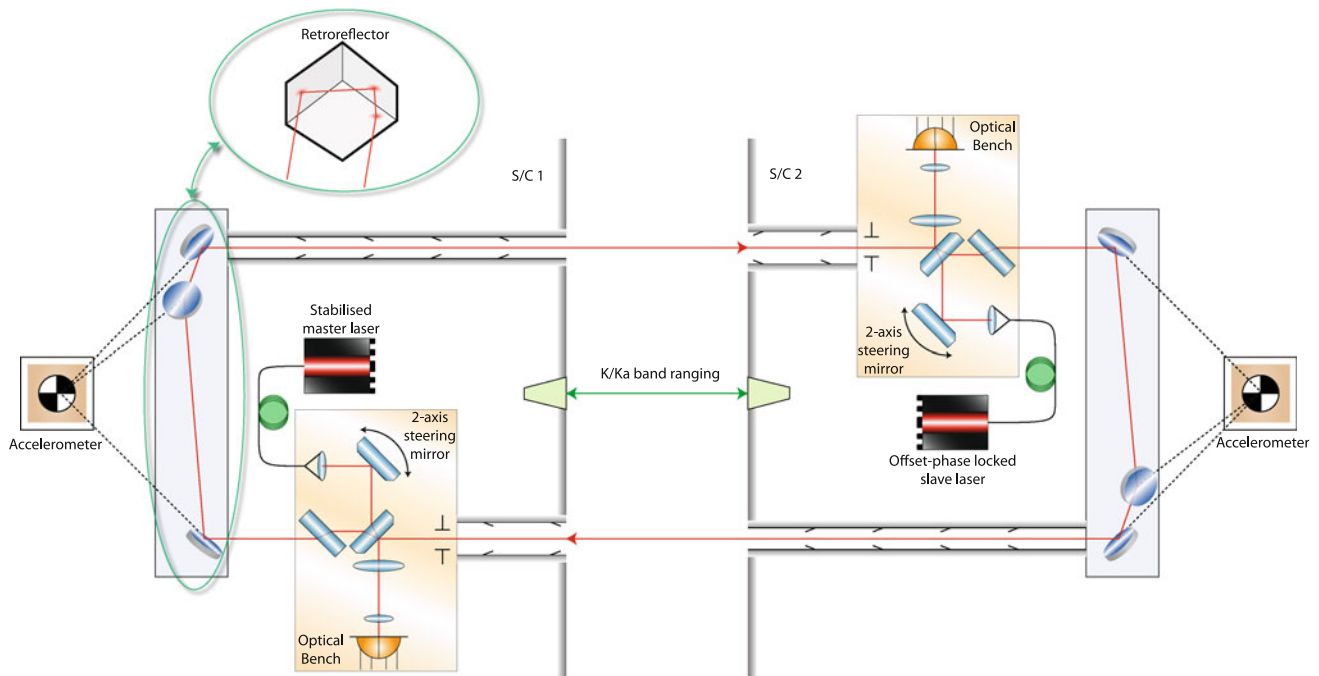


Fig. 1 Proposed optical layout for the laser ranging instrument (laser frequency stabilisation subsystem not shown). The microwave ranging system is labeled ‘K/Ka band ranging’ and is centered on axis

be located outside the mirror device, allowing the effective fiducial measurement point to be placed inside the accelerometer housing or the center of mass of the satellites. In addition, a number of important parameters are invariant under rotation around the intersection point (provided there are reflections from all three surfaces), namely:

- The round-trip pathlength is twice the distance between the beam starting point and a plane normal to the beam direction and intersecting the retro-reflector vertex.
- The propagation direction of the reflected beam is always anti-parallel to the incident beam.
- The lateral beam offset from the axis parallel to the incident ray but passing through the retro-reflector vertex is the same for both the incident and reflected rays.

These properties allow the system to maintain high immunity to spacecraft attitude jitter, even with off-axis beams.

For satellite separations of a few hundred kilometers a passive retroreflector is not feasible and an active transponder is required. One of the consequences of an active transponder is that without active beam steering spacecraft attitude errors will lead to misalignment between the received beam and the beam transmitted back to the other spacecraft since the outgoing beam direction would be fixed with respect to the transmitting spacecraft. The resulting misalignment would lead to a reduction in contrast to the local heterodyne signal and to pointing errors of the transmitted beam that reduce the power received at the distant spacecraft. If the satellite

attitude was sufficiently controlled then this misalignment might be tolerable. However, for GRACE-like pointing fluctuations of up to 4 mrad (Herman et al. 2004) active beam steering will be necessary.

In contrast to the GRACE microwave ranging system which uses dual one-way measurements, the basic LRI architecture consists of an offset phase-locked transponder. This enables the heterodyne frequencies to be conveniently controlled (except for the Doppler shifts which are determined by the relative spacecraft velocity) and kept within the measurement bandwidth. Offset phase locking with high gain/bandwidth eliminates the laser frequency noise of the transponder and any remaining residual is measured by the local phase measurement.

The offset phase-locked transponder configuration is well known and demonstrated in laboratory experiments (see for e.g. Jeganathan and Dubovitsky (2000); Pierce et al. (2008)); however, to authors’ knowledge it has not yet been demonstrated on orbit for intersatellite ranging. Some of the required technologies, e.g. phase locking without a frequency offset, have been demonstrated on orbit in intersatellite laser links for communication (Tolker-Nielsen and Oppenhaeuser 2002; Smutny et al. 2008, 2009); however, the architecture is fundamentally different.

3 Preliminary requirements

Figure 2 shows the preliminary requirements for the one-way ranging displacement noise in amplitude spectral density

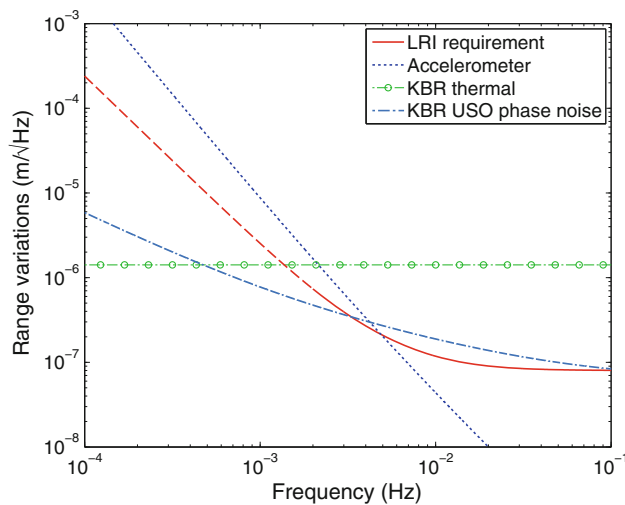


Fig. 2 Comparison between the proposed requirements (including margin) for the laser ranging instrument and the leading system noise terms for the GRACE microwave ranging system. The LRI requirement is shown as the solid red curve, whilst the dashed red curve for frequencies below 2 mHz is a goal. The dotted blue curve shows the equivalent ranging noise contribution from the GRACE accelerometers based on the nominal requirements. Also shown for comparison are estimates of the thermal noise and the USO phase noise (for the ‘worst case’ satellite separation of 270 km) contribution for the GRACE microwave ranging system

compared to the nominal performance requirement for the GRACE accelerometer and major contributions from the microwave K/Ka-band ranging (KBR) system. The dominant noise source for the KBR system is the thermal noise of the receiver, which depends on the SNR of the received signals. Also shown is the contribution from the ultra-stable oscillator (USO) phase noise to the ranging performance. The USO is used as a common frequency reference for the GPS receiver, the sampler used in the KBR system and is also used in the generation of the transmitted microwave beam. The requirement for the LRI shown in Fig. 2 is well below the contributions from both the accelerometer and the KBR system and corresponds to $80 \text{ nm}/\sqrt{\text{Hz}}$ (including margin) with relaxation towards low frequencies.

The overall performance at low frequencies will be limited by the accelerometer performance and the main improvement enabled by the LRI is in the 10 to 100 mHz frequency band, corresponding to spatial scales of 770 to 77 km for an orbital velocity of $\approx 7.7 \text{ km/s}$. For polar circular orbits the contribution of the zonal components of the gravitational field in the intersatellite range variation consists mainly of a tone whose frequency is equal to the coefficient order times the orbit frequency (Thomas 1999). Thus, the frequency band where the sensitivity of the laser instrument provides improved sensitivity corresponds approximately to zonal spherical harmonic coefficients of orders between 50 and 500. The signature of the sectoral coefficients is spread over a wider range and

also shifted towards lower frequencies compared to the zonal coefficients.

4 Measurement principle

Figure 3 shows a simplified sketch of the measured path-lengths. In the offset phase-locked transponder configuration the laser phase is controlled by feeding back the detected signal such that the beatnote phase on the transponder spacecraft $\psi_2(t)$ is driven to follow a linear ramp, i.e. $\omega_{\text{off}}t$. In this offset-locked condition the difference between the wavelengths of the two beams is very small and is neglected in this analysis. In the situation where the lengths are slowly varying compared to the light travel time between the spacecraft (which are in the order of 1 ms in this case) the intersatellite range to be measured is approximately

$$\rho(t) \approx \frac{1}{2} [x_1(t) + L_{12}(t) + y_2(t) + L_{21}(t) + x_2(t) + y_1(t)], \quad (1)$$

whereas the phase of the beatnote on the photodetector in S/C 1 can be written as

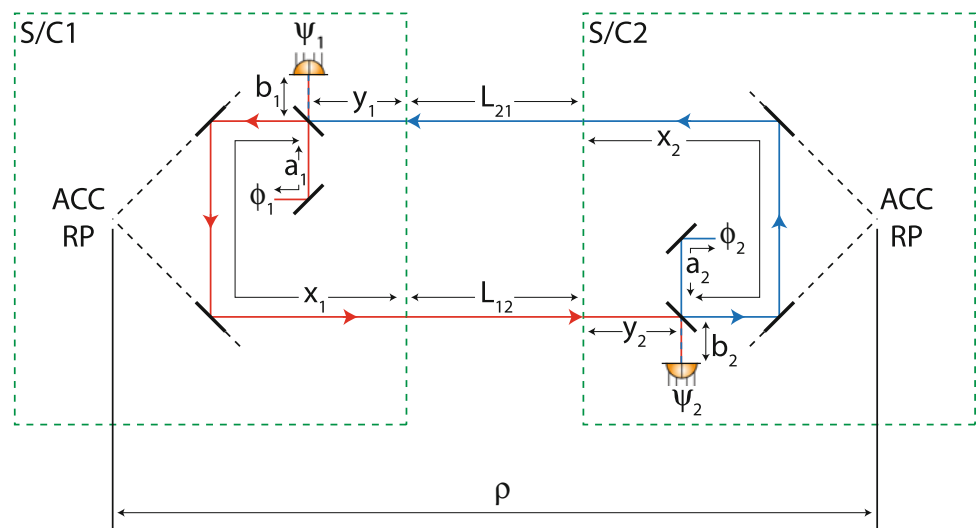
$$\psi_1(t) \approx -\omega_{\text{off}}t - [\varphi_1(t) - \varphi_1(t - \tau_{\text{rt}})] + k [a_1(t) - a_1(t - \tau_{\text{rt}})] - 2k\rho(t), \quad (2)$$

where $k = 2\pi/\lambda$, λ is the optical wavelength (the current baseline wavelength is 1,064 nm) and τ_{rt} is the round-trip travel time. The first term in Eq. 2 comes from the frequency offset used for offset phase locking and the second term leads to coupling of the laser phase noise. The third term, which has the same coupling factor as the laser phase noise is caused by changes of the pathlength from the laser to the beamsplitter on the master spacecraft and is negligible compared to the contribution from laser phase noise. The last term is proportional the desired fluctuations of the intersatellite range. The beatnote phase is measured by a phasemeter (Shaddock et al. 2006; Ware et al. 2006). The phasemeter output scaled to yield equivalent one-way range variation is

$$s_1(t) = \frac{\lambda}{4\pi} \psi_1(t) \approx \rho(t) + \frac{\lambda}{4\pi} [\varphi_1(t) - \varphi_1(t - \tau_{\text{rt}})] + \frac{1}{2} [a_1(t - \tau_{\text{rt}}) - a_1(t)] \quad (3)$$

and corresponds to the desired range measurement, $\rho(t)$, plus noise terms due to laser phase noise at the main beamsplitter on the master spacecraft. Like the microwave ranging system on GRACE, the absolute range is not measured because of the ambiguity for the initial phase measurement of an arbitrary number of integer wavelengths. The phase variations after the initial measurement point are, however, tracked continuously.

Fig. 3 Simplified sketch of the measured lengths for the proposed ‘racetrack’ configuration. *Red lines* indicate the lower laser frequency and *blue lines* the higher laser frequency. The configuration measures changes of the round-trip distance corresponding to 2ρ , twice the distance between the accelerometer reference points (labelled *ACC RP*)



An advantage of the proposed configuration is that to first order not only the lengths a_1 , a_2 , b_1 and b_2 but also the movement of the optical bench along the beam path cancel, since a change in the pathlength for the receive beam is cancelled by a corresponding change in the transmit path (e.g. x_1 and y_1 in Fig. 3). This significantly relaxes the dimensional stability requirements for the optical bench and its mounting.

5 Doppler shifts

The Doppler shift is related to the relative velocity of the spacecraft. The non-relativistic one-way Doppler frequency shift is given by

$$f_D \approx -\frac{v_{\text{rel}}}{\lambda}, \quad (4)$$

where v_{rel} is defined such that positive values correspond to an increasing separation between the satellites and a negative Doppler shift (i.e. red-shifted). For the proposed offset phase-locked transponder configuration the frequency of the heterodyne signals on the transponder photodetector is maintained at a chosen offset by feedback to the slave laser. The Doppler shift occurs in both directions such that the heterodyne frequency on the master spacecraft is the transponder offset plus twice the one-way Doppler shift (as can be seen in Eq. 2). The photodetector and phasemeter bandwidths must be sufficient to measure the heterodyne frequencies on both spacecraft. For relative velocities in the order of a few meters per second the one-way Doppler shifts correspond to a few megahertz for an operating wavelength of 1,064 nm. A relativistic analysis of the Doppler shifts results in a second order correction for Eq. 4 of order $v_{\text{rel}}/c \sim 10^{-8}$.

6 Optical bench

Figure 4 shows a schematic of the proposed optical bench. This optical bench would be rigidly mounted to the main equipment platform of the spacecraft. The light from the laser is delivered to the optical bench by an optical fibre. A small fraction of the light is split off before the optical bench using a fibre power splitter and directed to the frequency stabilisation subsystem. The fibre injector collimates and shapes the beam coming out of the fibre such that a beam waist of the desired size is generated on the steering mirror. The steering mirror must be able to rotate in two axes, i.e. produce tip and tilt. The beam is then directed to the beamsplitter

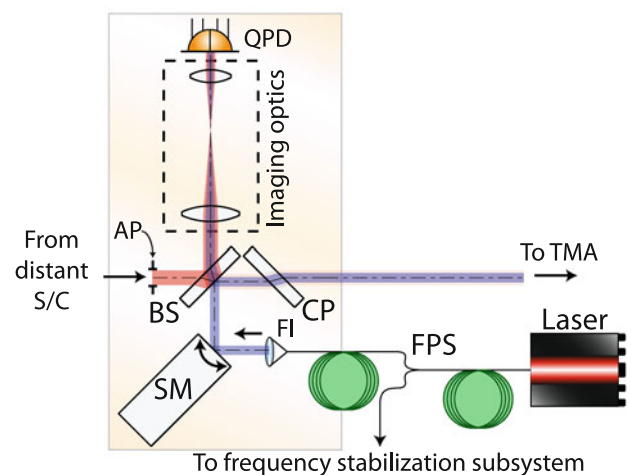


Fig. 4 Proposed optical bench layout. The local beam waist is located on the steering mirror. *AP* aperture, *BS* beamsplitter, *CP* compensation plate, *FI* fibre injector, *FPS* fibre power splitter, *QPD* quadrant photodetector, *SM* steering mirror

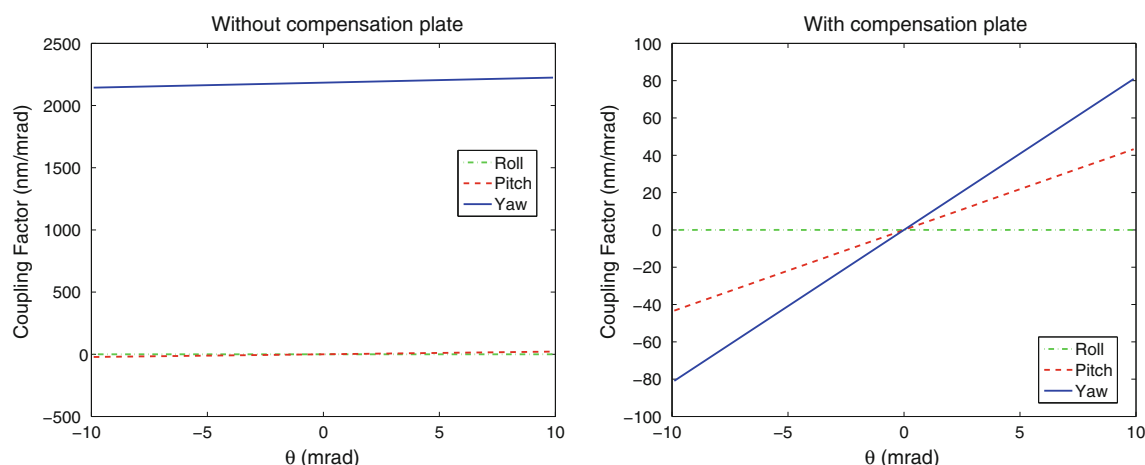


Fig. 5 Coupling factors for pitch, yaw and roll into the sensitive pathlength for only the beamsplitter (shown on the *left*) and for both the beamsplitter and compensation plate (shown on the *right*)

which has a high reflectivity such that most of the light is directed towards the distant spacecraft and a small fraction is transmitted and passes through a lens system before being detected on the quadrant photodetector where it is used as the local oscillator or reference beam.

The function of the lens system is to simultaneously image both the receive aperture and the local beam waist on the steering mirror onto the photodetector surface such that a beam tilt at either the aperture or the steering mirror leads to a pure tilt (i.e. without beam walk) on the photodetector. In addition, the imaging system will be used to match the beam size to the quadrant photodetector. Figure 4a shows a simple two-lens telescope (labeled “imaging optics”) for this purpose; however, other implementations are possible.

To achieve the correct imaging for both beams, the steering mirror and the aperture on the optical bench must have the same distance from the lens system. Aberrations present in this imaging system are largely common to both the local and the incoming beams which reduces the coupling from beam tilt into the differential phase measurement caused by these aberrations. The remaining residual coupling is mainly caused by the different spatial profile of the two beams and residual beam misalignments.

The pathlength through the beamsplitter is angle dependent which leads to a coupling of the spacecraft attitude jitter into the round-trip length measurement. The coupling factor for yaw is dominant and has been estimated to be on the order of $2.2 \mu\text{m}/\text{mrad}$ for a 7-mm thick fused silica beamsplitter. For pitch the coupling factor is quadratic and nominally at a turning point. These coupling factors as a function of spacecraft rotation are shown in Fig. 5.

To reduce the coupling from angle into measured pathlength, a compensation plate made from the same material as the main beamsplitter but rotated by 90° could be used. This

shifts the coupling factor for yaw also to a nominal minimum working point. The coupling factor with a 1 mrad error from the nominal minimum has been estimated to 10 nm/mrad with the compensation plate. These coupling factors were estimated using simple ray tracing along the sensitive path of the interferometer and for nominally perfect geometry. More detailed simulations using propagation of non-Gaussian beams are being developed. An alternative solution would be to use a cube beamsplitter.

7 Satellite pointing

The orientation of the GRACE satellites is controlled using three magnetic torque rods and additionally using six pairs of cold gas thrusters when the Earth’s magnetic field lines are unfavourably aligned or if the disturbances are such that the magnetic torque rods have insufficient control authority (Herman et al. 2004). Whilst this level of attitude control is sufficient for the microwave ranging system due its lower beam divergence and wider receive field of view, the angular fluctuations are too large for the laser interferometer. Consequently, measurement and active control of beam pointing will be required.

In future gravity field missions, the required pointing accuracy could be potentially achieved by improved spacecraft pointing control, however, for the demonstration instrument discussed here, the pointing control must be implemented internally in the instrument itself. To implement pointing control both a sensor and a actuation mechanism are required. These are discussed in the following sections.

Beam pointing control does not eliminate the coupling of spacecraft jitter completely from the measurement. For e.g. an offset of the triple mirror vertex from the accelerometer

reference point leads to a coupling of satellite attitude jitter into the measured round-trip length variations. For a retro-reflector with perfect 90° angles the linearised dependence of the measured round-trip pathlength as a function of offsets from the accelerometer reference point can be written as:

$$\delta L_{rt} \approx 2(\Delta x \theta_y - \Delta z) \delta \theta_y + 2(\Delta x \theta_z + \Delta y) \delta \theta_z, \quad (5)$$

where Δx , Δy , and Δz are the offsets in the along-track, cross-track and radial direction, respectively. The angles θ_y and θ_z are the infinitesimal rotations around the y and z axes, respectively (i.e. pitch and yaw angles). For example, lateral offsets (Δy and Δz) of $100 \mu\text{m}$, a longitudinal offset (Δx) of 1 cm , static pointing error of 1 mrad and a pointing noise of $100 \mu\text{rad}/\sqrt{\text{Hz}}$ contributes $16 \text{ nm}/\sqrt{\text{Hz}}$ of one-way pathlength noise per spacecraft. The requirements on these offsets depend on the ultimate attitude and orbit control system performance. Misaligned mirrors also lead to coupling from angular jitter, however, the static mirror alignments are driven by the static pointing error requirements. Notice that Eq. 5 does not depend on roll. However, imperfections in alignment of the mirror planes can also lead to a coupling for roll into the measured round-trip length variations.

8 Differential wavefront sensing

Differential wavefront sensing (DWS) is a well-known technique for measuring the relative wavefront misalignment between two beams with high sensitivity (see for e.g. Anderson (1984); Morrison et al. (1994a,b); Heinzel et al. (1999a,b, 2004)). Figure 6 illustrates the basic principle of DWS. Two beams with a relative misalignment and frequency offset are detected using a quadrant photodetector. The phase of the resulting beatnote of the detector is measured separately on each element. For the situation shown in Fig. 6 the average phase on one half of the detector is equal in magnitude to that on the other half but has the opposite sign. For small misalignments the relative phase shift between the two beatnotes is proportional to the misalignment. Neglecting the heterodyne amplitude variations across the photodiode surface, the average phase difference between the signals on the two halves of the detector for two flat-top beams of equal radius can be approximated for infinitesimally small tilts by:

$$\Delta\theta \approx \frac{16r}{3\lambda} \alpha, \quad (6)$$

where α is the relative wavefront tilt, r the beam radius and λ is the optical wavelength.

The situation for the optical bench is more realistically modelled by interference between a Gaussian and a flat-top beam for which the DWS signals can be computed numerically. The conversion factor between wavefront tilt (α) and the DWS signal for typical beam parameters is large, for e.g. if $r = 4 \text{ mm}$ and $\lambda = 1,064 \text{ nm}$ then the conversion

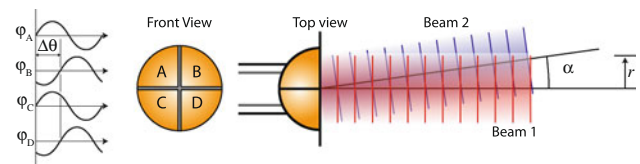


Fig. 6 Differential wavefront sensing principle. Two beams of radius r with a relative wavefront tilt of α are detected by a quadrant photodetector. The two beams also have a slight frequency difference

factor in Eq. 6 is approximately $20,000 \text{ rad/rad}$. In addition, many noise sources and signals present in the longitudinal signal are common and thus cancel in the DWS signals, e.g. laser frequency noise and pathlength fluctuations. Consequently, the combination of large conversion factor and low noise enable very precise measurements of relative wavefront tilt.

In this case the relative wavefront tilt represents the deviation between the propagation axes of the received beam and the local beam. Since the alignment of the optical bench with respect to the spacecraft is nominally static the DWS signals are related to the local spacecraft pointing errors relative to the intersatellite axis. Provided that care is taken to minimise (or calibrate) phase offsets between the channels in the phase measurement system, then zeroing the DWS signals corresponds to optimum alignment and maximum contrast for the interferometer. This also corresponds to the optimal alignment for the transmit beam provided that the TMA, beamsplitter and compensation plate do not introduce significant additional misalignment. The DWS signals measured on each spacecraft therefore can be used as error signals for a feedback control system to control not only the local beam alignment but also optimal pointing of the transmit beam towards the other spacecraft such that it matches that of the incoming beam even in the presence of spacecraft attitude jitter.

Using quadrant photodetectors as shown in Fig. 6 allows simultaneous measurement of relative wavefront tilt in two axes (in addition to the longitudinal signal) by forming the following combinations:

$$\bar{\theta}_T - \bar{\theta}_B = \left(\frac{\varphi_A + \varphi_B}{2} \right) - \left(\frac{\varphi_C + \varphi_D}{2} \right) \quad (7)$$

$$\bar{\theta}_L - \bar{\theta}_R = \left(\frac{\varphi_A + \varphi_C}{2} \right) - \left(\frac{\varphi_B + \varphi_D}{2} \right), \quad (8)$$

where φ_A , φ_B , φ_C and φ_D are the phases for the heterodyne signals on each of the quadrants according to the arrangement shown in Fig. 6. The longitudinal signal can also be obtained simultaneously by averaging the phases on each quadrant:

$$\varphi_L = \frac{\varphi_A + \varphi_B + \varphi_C + \varphi_D}{4}. \quad (9)$$

Additionally, a weighted average where the weights are the relative signal amplitudes of each quadrant could also be

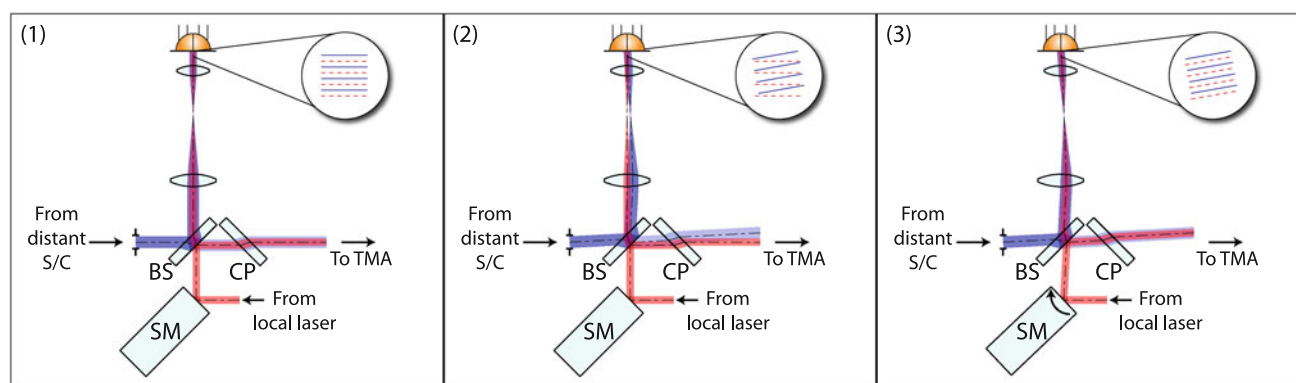


Fig. 7 Function of the steering mirror control loop. From left to right: (1) nominal situation with spacecraft perfectly aligned, (2) spacecraft misalignment produces a non-zero DWS signal on the photodetector, (3)

feedback to steering mirror makes DWS signal zero and makes outgoing beam parallel to incoming beam. SM steering mirror, BS beamsplitter, CP compensation plate

used to improve the statistics. Thus, the three main signals derived from the phase measurements of the quadrant photodetector outputs are the two differential wavefront sensing signals and the longitudinal signal which contains phase variations proportional to the changes in intersatellite range.

9 Steering mirror control and interferometer pointing data

As the instrument is a demonstration instrument it will not be possible to use the DWS signals to control the satellite attitude to optimise the interferometer contrast by driving the DWS signal to zero. Instead, the instrument must internally compensate for the angular fluctuations induced by spacecraft attitude jitter. One possible implementation would be to actuate the orientation of the entire optical bench which has the advantage that the optical path is always centred in the beam compressor. A potential concern with moving components is a possible negative effect on the sensitive accelerometer. However, this effect has been estimated to be below the sensitivity of the accelerometer (Folkner et al. 2010). The proposed alternative is to use a steering mirror which moves much less mass and allows for a higher actuation bandwidth which could reduce the time required for link acquisition. Another advantage of a steering mirror is that a standard component could be used either as is or with minimal changes.

Figure 7 illustrates the principle of operation of the steering mirror control loop. Three situations are shown. The first is the nominal situation where the incoming beam and the local beam are aligned. The illustration in the middle shows the situation when the spacecraft alignment changes, leading to a non-zero DWS signal and also a misalignment between the incoming and outgoing beam. The misalignment in this situation leads to a reduction in the heterodyne efficiency (signal strength) on the local photodetector and also

misalignment of the transmitted beam and consequently a reduction power received by the distant satellite. Implementing the steering mirror control loop zeros the DWS signal by rotating the steering mirror such that the local and incoming beams have the same alignment on the photodetector (shown on the right of Fig. 7). As a result, both the interference contrast is optimised and even more importantly the outgoing beam is made parallel to the incoming beam such that it points back to the other spacecraft independently of the local spacecraft orientation. The local spacecraft can thus be considered an ‘active retroreflector’.

Ideally, the beam pointing is controlled by the steering mirror control loop such that the error signal derived from DWS is close to zero. In order to derive the pointing information for further analysis or noise reduction (analogous to the phase center correction applied to the KBR data), the raw DWS signal itself cannot be used in this case and the pointing information can instead be derived from the steering mirror commanded angles.

Both the steering mirror and the optical bench pointing concepts have the advantage that to first order the length stability of the angular actuator does not couple into the measured pathlength, significantly relaxing the longitudinal stability requirements for the mechanism. Motion of the steering mirror which couples into the final measurement via time of flight effects as discussed in Sect. 4 effectively produces a Doppler shift of the light; however, this is negligible compared to the stabilised laser frequency noise.

10 Interferometer noise sources

For the LRI performance the two dominant noise sources expected are pointing-induced noise and laser frequency noise. Pointing-induced noise has been discussed in Sects. 6–9. Equation 3 shows the coupling of laser phase noise into

the ranging measurement. The equivalent coupling factor for laser frequency noise can be expressed as

$$\tilde{\delta x} \approx \frac{\rho}{\nu} \tilde{\delta \nu}, \quad (10)$$

where $\tilde{\delta \nu}$ is the linear spectral density of the laser frequency noise, ν the laser frequency and $\tilde{\delta x}$ is the resulting ranging noise. This coupling factor can be derived from equation 3 by converting the term due to laser phase noise into the frequency domain and rewriting in terms of laser frequency noise:

$$\begin{aligned} \tilde{\delta x} &= \frac{\lambda}{4\pi} |1 - \exp(-j2\pi f \tau_{\text{rt}})| \frac{\tilde{\delta \nu}}{f} \\ &\approx \frac{\lambda \tau_{\text{rt}}}{2} \tilde{\delta \nu} \quad (f \ll \tau_{\text{rt}}^{-1}) \\ &\approx \frac{\rho}{\nu} \tilde{\delta \nu}. \end{aligned} \quad (11)$$

Hence, the coupling of laser frequency noise into the range measurement is proportional to the satellite separation, ρ . The analog of laser frequency noise in the GRACE KBR system is the USO phase noise which is also shown in Fig. 2 for comparison. Assuming that the evolution of the spacecraft separation will be comparable to that of GRACE the worst case is $\rho = 270$ km. A stabilised frequency noise level of $30 \text{ Hz}/\sqrt{\text{Hz}}$, as also proposed for LISA, therefore corresponds to $30 \text{ nm}/\sqrt{\text{Hz}}$ for a laser frequency of 281 THz ($\lambda = 1,064 \text{ nm}$) and represents a substantial fraction of the LRI ranging requirement.

A common technique to stabilise the laser frequency is to lock the laser to a resonance of a reference cavity housed in a thermally stable environment using an RF modulation and detection scheme (Drever et al. 1983; Black 2001). Using this technique frequency stability better than the $30 \text{ Hz}/\sqrt{\text{Hz}}$ level has been achieved in laboratory experiments (Tröbs 2005; Ludlow et al. 2007; Alnis et al. 2008). A space qualified version of such a frequency stabilisation system for a GRACE follow-on mission is under development (Folkner et al. 2010, 2011). Although only one laser frequency stabilisation subsystem (which is not shown in Fig. 1 for simplicity) is required, it can be included on both spacecraft for redundancy and allows either spacecraft to be used as the master or the transponder, with the function selectable by telecommand.

Pointing-induced noise can be caused by offsets of the retro-reflector vertex from the accelerometer reference point (located at the center-of-mass of the spacecraft), phase changes due to beam walk effects and far-field curvature errors.

Optical pathlength variations unrelated to the changes caused by gravitational forces, for e.g. due to thermal effects, lead to measurement error. The thermal variations are expected to have significant quasi-periodic variations

corresponding to the orbit frequency and its harmonics. Since the signal of interest is also concentrated in tones corresponding to harmonics of the orbit frequency (Thomas 1999) the dimensional stability of components in the sensitive optical path is most critical. An advantage of the proposed design is that the main sensitive path contains only a few components. The dimensional stability of the other components not in the sensitive path only couples via second order effects. This relaxes the length stability requirements for the steering mirror and imaging optics.

Readout noise is predicted to be well below the other noise sources and includes:

- USO noise,
- shot noise,
- laser power noise,
- photodetector electronic noise,
- parasitic signals (e.g. scattered light and electronic cross-talk),
- analog-to-digital converter quantisation noise,
- spurious electronic phaseshifts.

The USO noise couples into the measurement as it is used as the reference for the sampler to readout the photodetector signals. The USO phase noise results in sampling time errors which lead to frequency-dependent phase errors that are proportional to the beatnote frequency.

The contribution from shot noise is inversely proportional to the square-root of the effective power of the received beam and is negligible for the power levels under consideration.

The effect of photodetector electronic noise depends on the power used in the local oscillator beam and thus can be made negligible compared to other contributions by selecting the appropriate beam power. In order to minimise the incoming signal power required for acquisition the local beam power level should be chosen high enough such that photodetector electronic noise is below or comparable to the shot noise limit. The effect of laser power noise, on the other hand, can be mitigated by decreasing the local oscillator beam power, thus there is an optimal value for the local oscillator power. Due to the frequency dependence of laser power noise and photodetector electronic noise the optimal local oscillator power is dependent on the heterodyne frequency used.

Spurious electronic phaseshifts, e.g. temperature- or stress-dependent phase shifts in cables, can be mitigated with appropriate design and choice of materials. Parasitic signals are analogous to the multipath effect in the microwave ranging system and can be caused by ghost beams, electrical cross coupling, etc. These can be problematic if they lead to signals at the same frequency as the main beatnote. Experiments and simulations are under way.

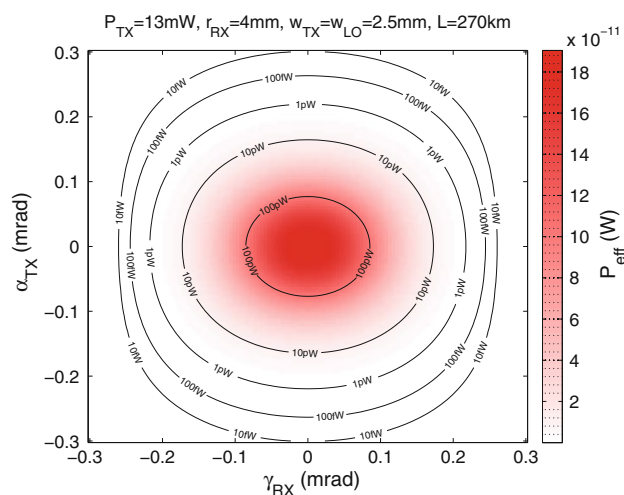


Fig. 8 Effective power for the sum of all four photodetector quadrants as a function of transmitter (α_{TX}) and receiver (γ_{TX}) pointing error

Table 1 Parameter used for computation of the effective received power

Parameter	Value	Units
Laser power	25	mW
Laser wavelength	1,064	nm
Satellite separation	270	km
Receive aperture radius	4	mm
Transmit beam waist radius	2.5	mm
Transmission efficiency for receive path	97	%
Transmit efficiency	50	%
Transmit efficiency	50	%

The value for the ‘Transmission efficiency for receive path’ parameter includes the reflection from the beamsplitter and loss in the imaging optics, but neither the photoreceiver efficiency nor the heterodyne efficiency. The heterodyne efficiency is, however, included in the effective power computation. The small loss caused by the gap between the quadrants has been neglected in the analysis presented here. The ‘Transmit efficiency’ includes the fibre power splitter, transmission through the components on the optical bench and the TMA

11 Link power budget

To first order for a small receive aperture compared to the beam spot size at the receiving satellite the total received power depends on the alignment of the transmitter and the aperture size, whilst the receiver alignment determines the contrast and thus the effective received power. Figure 8 shows the simulated effective power for the parameters given in Table 1. Even with the largest expected intersatellite distance of 270 km more than 100 pW of effective power is received for beam pointing errors of 50 μ rad or less. Note that the pointing error in Fig. 8 is the *beam* pointing error and not that of the spacecraft since the beam pointing error is determined by the effectiveness of the steering mirror control loop and the special properties of the triple mirror assembly.

12 Instrument calibration and validation

The fundamental measurement is derived from the optical phase variations observed at the master spacecraft which corresponds to the round-trip length variations. The intersatellite range variations are therefore obtained by:

$$\delta\rho(t) = k \frac{\delta\psi_1(t)}{2} = \frac{\lambda}{4\pi} \delta\psi_1(t). \quad (12)$$

Thus, the primary calibration of the range variations is via the accurate knowledge of the optical wavelength. If the laser frequency is known with an accuracy of a few Gigahertz the corresponding wavelength knowledge is approximately 1 part in 10^5 . Once operating, the distance changes can be tracked over many wavelengths (limited only by the associated Doppler shifts and counter bit-depth). There is, however, a constant offset because of the initial unknown integral number of wavelengths. This can be treated as a parameter to be estimated in the data processing step.

Verifying the noise level without the presence of an independent measurement system of equal precision is particularly challenging. Simultaneous operation of the laser ranging and the microwave ranging system allows for cross comparison between the two systems which should at least allow verification of the system noise at the KBR level of precision and also permit identification of possible systematic effects¹ in each system, provided they are not common. The methods used to validate the gravitational fields from GRACE, such as comparison with terrestrial gravity data, GPS leveling, ocean bottom pressure or hydrological models, may also be used for the solutions obtained using the laser ranging data. In addition, the precise pointing information provided by the interferometer opens new possibilities for cross-comparison, noise correlation and removal.

13 Point-ahead angle

Due to the finite light travel time and the fact that the spacecraft are moving relative to each other there is an angular difference between the optimal transmit and receive angles. In a simplified picture the transmit beam must be directed to where the distant satellite will be in the time taken for the light to propagate between the spacecraft, whilst the receiver must be oriented to where the distant spacecraft was before in the time taken to travel from the distant spacecraft. If the time varying component of this angular difference is significant an actuator may be needed to compensate. In a non-relativistic analysis and for small angles the point-ahead angle is

¹ The possible presence of unmodelled effects in the microwave ranging data has been suggested in Kim and Lee (2009).

approximately (McElroy et al. 1977):

$$\theta_{p.a.} \approx \frac{2v_{\perp}}{c}, \quad (13)$$

where c is the speed of light and v_{\perp} is the component of the relative velocity of the two spacecraft perpendicular to the line-of-sight (i.e. the line connecting the two centers of mass of the two spacecraft).

For GRACE-like orbits and also pendulum orbits² with modest rotation between the two orbital planes the dominant component is caused by the rotation of the line-of-sight by a full revolution once per orbit and is approximately constant with an order of magnitude of approximately $2 \mu\text{rad}$. Unlike intersatellite laser links for communication (Tolker-Nielsen and Oppenhaeuser 2002; Smutny et al. 2008, 2009) and the future LISA space-based gravitational wave detector (Danzmann and the LISA Science Team 2003; Danzmann and Rüdiger 2003; Heinzel et al. 2006; Shaddock 2008) active compensation should not be necessary.

14 Sagnac effect

Since the two counter-propagating beams are spatially separated the area enclosed is not zero. This leads to a change in the round-trip phase shift and correspondingly equivalent round-trip length of

$$\Delta x_{\text{rt}} = \frac{\lambda}{2\pi} \times \Delta \phi_{\text{rt}} = \frac{A\Omega}{c} \quad (14)$$

where A is the enclosed area, Ω the rotation rate around the normal of the plane and c is the speed of light. The enclosed area for the proposed configuration is approximately $A \approx 2 \times 10^5 \text{ m}^2$. For GRACE-like orbits the rotation rates around the normal to the plane are nominally zero. However, for pendulum orbits there is an approximately sinusoidal variation of the line of sight in the plane with a period corresponding to the orbit period. The effect on the recovered gravitational field should therefore be minimal since the gravity field signal energy is concentrated in the frequency band above the orbital frequency. Additionally, the amplitude of the Sagnac effect is small for the orbits under consideration and the effect can be modelled using Eq. 14.

² The pendulum orbit configuration is similar to the GRACE configuration but the orbit planes of the two satellites are rotated slightly around the North–South axis (Krieger et al. 2003). In terms of Keplerian elements the satellites have differing right ascensions of the ascending node, leading to a cross-track separation between the satellites when the constellation is at the equator but no cross-track separation when the constellation is at the poles.

15 Link acquisition

Establishing the laser link between two satellites is challenging, particularly on the first attempt as there are unknown biases between the star tracker alignment and the interferometer ‘boresight’ (corresponding to DWS zero) due to manufacturing tolerances and structural deformations experienced during/after launch. Once the alignment bias between the star tracker and the interferometer has been calibrated subsequent reacquisition attempts will have a reduced search space whose size will depend on the accuracy and stability of the calibration. During nominal operation the bias can be continuously monitored by comparing the star tracker measurement with the signal applied to the steering mirror. This strategy requires that the steering mirror alignment be accurately measured by independent or internal sensors (e.g. strain gauges or capacitive sensors). These internal sensor signals could either be maintained close to zero by a control loop or alternatively recorded. The acquisition strategy will be presented in a subsequent paper.

16 Summary and future work

A laser interferometer for intersatellite ranging that can operate in parallel with the microwave ranging system of a future GRACE follow-on mission has been presented. Experimental demonstration of the basic concept is in progress and further detailed analysis is ongoing. This interferometer is intended to demonstrate key technologies required for the next generation of gravity field missions based on intersatellite ranging. Simultaneous operation of this laser ranging system with the microwave ranging system presents a unique opportunity to study the performance of both instruments.

Acknowledgements This work was partly funded by the “Deutsche Forschungsgemeinschaft” (DFG) within the Cluster of Excellence QUEST (Centre for Quantum Engineering and Space-Time Research). Parts of the research described in this publication were carried out at the Jet Propulsion Laboratory, California Institute of Technology, under a contract with the National Aeronautics and Space Administration. This work was also supported under the Australian Government’s Australian Space Research Program.

References

- Alnis J, Matveev A, Kolachevsky N, Udem T, Hänsch TW (2008) Subhertz linewidth diode lasers by stabilization to vibrationally and thermally compensated ultralow-expansion glass Fabry-Pérot cavities. *Phys. Rev. A* 77:053809
- Anderson DZ (1984) Alignment of resonant optical cavities. *Appl Opt* 23(17):2944
- Bender PL, Wiese DN, Nerem RS (2008) A possible dual-GRACE mission with 90 degree and 63 degree inclination orbits. In:

- Proceedings of the 3rd International Symposium on Formation Flying, Missions and Technologies
- Bertiger W, Bar-Sever Y, Desai S, Dunn C, Haines B, Kruizinga G, Kuang D, Nandi S, Romans L, Watkins M, Wu S, Bettadpur S (2002) GRACE: Millimeters and Microns in Orbit. In: Proc ION GPS 2002
- Black ED (2001) An introduction to Pound–Drever–Hall laser frequency stabilization. *Am J Phys* 69(1):79–87
- Danzmann K, Rüdiger A (2003) LISA technology–concept, status, prospects. *Class Quantum Gravity* 20:S1
- Danzmann K, the LISA Science Team (2003) LISA: An ESA cornerstone mission for the detection and observation of gravitational waves. *Adv Space Res* 32(7):1233–1242
- Drever RWP, Hall JL, Kowalski FV, Hough J, Ford GM, Munley AJ, Ward H (1983) Laser phase and frequency stabilization using an optical resonator. *Appl Phys B* 31(2):97–105
- Dunn C, Bertiger W, Bar-Sever Y, Desai S, Haines B, Kuang D, Franklin G, Harris I, Kruizinga G, Meehan T, Nandi S, Nguyen D, Rogstad T, Thomas JB, Tien J, Romans L, Watkins M, Wu SC, Bettadpur S, Kim J (2003) Instrument of Grace: GPS augments gravity measurements. *GPS World* 14:16–28
- Folkner WM, de Vine G, Klipstein WM, McKenzie K, Shaddock D, Spero R, Thompson R, Wuchenich D, Yu N, Stephens M, Leitch J, Davis M, de Cino J, Pace C, Pierce R (2010) Laser frequency stabilization for GRACE-II. In: Proceedings of the 2010 Earth Science Technology Forum
- Folkner WM, de Vine G, Klipstein WM, McKenzie K, Spero R, Thompson R, Yu N, Stephens M, Leitch J, Pierce R, Lam TTY, Shaddock DA (2011) Laser frequency stabilization for GRACE-2 In: Proceedings of the 2011 Earth Science Technology Forum
- Heinzel G, Rüdiger A, Schilling R, Strain K, Winkler W, Mizuno J, Danzmann K (1999) Automatic beam alignment in the Garching 30-m prototype of a laser-interferometric gravitational wave detector. *Opt Commun* 160:321–334
- Heinzel G, Rüdiger A, Schilling R, Strain K, Winkler W, Mizuno J, Danzmann K (1999) Corrigendum to “Automatic beam alignment in the Garching 30-m prototype of a laser-interferometric gravitational wave detector” [*Opt. Commun.* 160 (1999) 321–334]. *Opt Commun* 164:161
- Heinzel G, Wand V, García A, Jennrich O, Braxmaier C, Robertson D, Middleton K, Hoyland D, Rüdiger A, Schilling R, Johann U, Danzmann K (2004) The LTP interferometer and phasemeter. *Class Quantum Gravity* 21:S581–S587
- Heinzel G, Braxmaier C, Danzmann K, Gath P, Hough J, Jennrich O, Johann U, Rüdiger A, Sallusti M, Schulte H (2006) LISA interferometry: recent developments. *Class Quantum Gravity* 23:S119
- Herman J, Presti D, Codazzi A, Belle C (2004) Attitude Control for GRACE: The first low-flying satellite formation. In: Proceedings of the 18th international symposium on space flight dynamics
- Horwath M, Lemoine JM, Biancale R, Bourgogne S (2011) Improved GRACE science results after adjustment of geometric biases in the Level-1B K-band ranging data. *J Geod* 85:23–38
- Jeganathan M, Dubovitsky S (2000) Demonstration of nm-level active metrology for long range interferometric displacement measurements. *Proc SPIE* 4006:838–846
- Kim J, Lee SW (2009) Flight performance analysis of GRACE K-band ranging instrument with simulation data. *Acta Astronautica* 65:1571–1581
- Knudsen P, Andersen O (2002) Correcting GRACE gravity fields for ocean tide effects. *Geophys Res Lett* 29:1178
- Krieger G, Fiedler H, Mittermayer J, Papathanassiou K, Moreira A (2003) Analysis of multistatic configurations for spaceborne SAR interferometry. *IEE Proc Radar Sonar Navig* 150:87
- Loomis BD, Nerem RS, Luthcke SB (2011) Simulation study of a follow-on gravity mission to grace. *J Geodesy* 1–17. <http://dx.doi.org/10.1007/s00190-011-0521-8>, doi:10.1007/s00190-011-0521-8
- Ludlow AD, Huang X, Notcutt M, Zanon-Willette T, Foreman SM, Boyd MM, Blatt S, Ye J (2007) Compact, thermal-noise-limited optical cavity for diode laser stabilization at 1×10^{-15} . *Opt Lett* 32(6):641
- McElroy JH, McAvoy N, Johnson EH, Degnan JJ, Goodwin FE, Henderson DM, Nussmeier TA, Stokes LS, Peyton BJ, Flattau T (1977) CO₂ Laser communication systems for near-earth space applications. *Proc IEEE* 65(2):221
- Morrison E, Meers BJ, Robertson DI, Ward H (1994) Automatic alignment of optical interferometers. *Appl Opt* 33(22):5041–5049
- Morrison E, Meers BJ, Robertson DI, Ward H (1994) Experimental demonstration of an automatic alignment system for optical interferometers. *Appl Opt* 33(22):5037–5040
- Pierce R, Leitch J, Stephens M, Bender P, Nerem R (2008) Intersatellite range monitoring using optical interferometry. *Appl Opt* 47:5007–5018
- Schmidt R, Flechtner F, Meyer U, Neumayer KH, Dahle C, Koenig R, Kusche J (2008) Hydrological signals observed by the GRACE satellites. *Surv Geophys* 29(4–5):319–334
- Seo KW, Wilson CR, Han SC, Waliser DE (2008) Gravity Recovery and Climate Experiment (GRACE) alias error from ocean tides. *J Geophys Res* 113:B03405
- Shaddock D, Ware B, Halverson PG, Spero RE, Klipstein B (2006) Overview of the LISA Phasemeter. *AIP Conf Proc* 873:654–660
- Shaddock DA (2008) Space-based gravitational wave detection with LISA. *Class Quantum Gravity* 25:114012
- Smutny B, Lange R, Kämpfner H, Dallmann D, Mühlnikel G, Reinhardt M, Saucke K, Sterr U, Wandernoth B, Czichy R (2008) In-orbit verification of optical inter-satellite communication links based on homodyne BPSK. *Proc SPIE* 6877:687702
- Smutny B, Kaempfner H, Muehlnikel G, Sterr U, Wandernoth B, Heine F, Hildebrand U, Dallmann D, Reinhardt M, Freier A, Lange R, Boehmer K, Feldhaus T, Mueller J, Weichert A, Greulich P, Seel S, Meyer R, Czichy R (2009) 5.6 Gbps optical intersatellite communication link. *Proc SPIE* 7199:719906
- Sneeuw N, Flury J, Rummel R (2005) Science requirements on future missions and simulated mission scenarios. *Earth Moon Planets* 94:113–142
- Tapley BD, Chambers DP, Bettadpur S, Ries JC (2003) Large scale ocean circulation from the GRACE GGM01 Geoid. *Geophys Res Lett* 30(22):2613
- Tapley BD, Bettadpur S, Ries JC, Thompson PF, Watkins MM (2004) GRACE measurements of mass variability in the Earth system. *Sci* 305:503–505
- Tapley BD, Bettadpur S, Watkins M, Reigber C (2004b) The Gravity Recovery and Climate Experiment: mission overview and early results. *Geophys Res Lett* 31(9):L09607
- Thomas JB (1999) An Analysis of Gravity-Field Estimation Based on Intersatellite Dual-1-Way Biased Ranging, JPL Publication, vol 98-15. Jet Propulsion Laboratory, Pasadena
- Thompson PF, Bettadpur SV, Tapley BD (2004) Impact of short period, non-tidal, temporal mass variability on GRACE gravity estimates. *Geophys Res Lett* 31:L06619
- Tiwari VM, Wahr J, Swenson S (2009) Dwindling groundwater resources in northern India, from satellite gravity observations. *Geophys Res Lett* 36:L18401
- Tolker-Nielsen T, Oppenhaeuser G (2002) In Orbit test result of an operational optical intersatellite link between ARTEMIS and SPOT4, SILEX. *Proc SPIE* 4635:1
- Touboul P, Willeminot E, Foulon B, Josselin V (1999) Accelerometers for CHAMP, GRACE and GOCE space missions: synergy and evolution. *Boll Geof Teor Appl* 40:321–327
- Tröbs M (2005) Laser development and stabilization for the spaceborne interferometric gravitational wave detector LISA. Ph.D. thesis, University of Hannover

- van den Broeke M, Bamber J, Ettema J, Rignot E, Schrama E, van de Berg WJ, van Meijgaard E, Velicogna I, Wouters B (2009) Partitioning Recent Greenland Mass Loss. *Science* 326:984–986
- Visser PNM, Sneeuw N, Reubelt T, Losch M, van Dam T (2010) Space-borne gravimetric satellite constellations and ocean tides: aliasing effects. *Geophys J Int* 181:789–805
- Ware B, Folkner WM, Shaddock D, Spero R, Halverson P, Harris I, Rogstad T (2006) Phase Measurement System for Inter-Spacecraft Laser Metrology. In: Proceedings of the 2006 Earth Science Technology Conference
- Wiese DN, Folkner WM, Nerem RS (2009) Alternative mission architectures for a gravity recovery satellite mission. *J Geod* 83:569–581
- Wouters B, Chambers D, Schrama EJO (2008) GRACE observes small-scale mass loss in Greenland. *Geophys Res Lett* 35:L20501
- Zenner L, Gruber T, Jäggi A, Beutler G (2010) Propagation of atmospheric model errors to gravity potential harmonics-impact on GRACE de-aliasing. *Geophys J Int* 182:797–807